THE JOURNAL OF PHYSICAL CHEMISTRY B

Article

pubs.acs.org/JPCB

Effect of High Pressure on the Typical Supramolecular Structure of Guanidinium Methanesulfonate

Shourui Li,[†] Qian Li,[†] Jing Zhou,[‡] Run Wang,[†] Zhangmei Jiang,[†] Kai Wang,[†] Dapeng Xu,[‡] Jing Liu,[§] Bingbing Liu,[†] Guangtian Zou,[†] and Bo Zou*[,†]

[†]State Key Laboratory of Superhard Materials and [‡]College of Physics, Jilin University, Changchun 130012, China

[§]Beijing Synchrotron Radiation Laboratory, Institute of High Energy Physics, Chinese Academy of Sciences, Beijing 100039, China

ABSTRACT: We report the high-pressure response of guanidinium methanesulfonate ($C(NH_2)_3^+ \cdot CH_3SO_3^-$, GMS) using in situ Raman spectroscopy and synchrotron X-ray diffraction (XRD) techniques up to the pressures of ~11 GPa. GMS exhibits the representative supramolecular structure of two-dimensional (2D) hydrogen-bonded bilayered motifs under ambient conditions. On the basis of the experimental results, two phase transitions were identified at 0.6 and 1.5 GPa, respectively. The first phase transition, which shows the reconstructive feature, is ascribed to the rearrangements of hydrogen-bonded networks, resulting in the symmetry transformation from *C*2/*m* to *Pnma*. The second one proves to be associated with local distortions of methyl groups, accompanied by the symmetry transformation from *Pnma* to $Pna2_1$. The cooperativity of hydrogen bonding, electrostatic, and van der Waals interactions, as well as mechanisms for the phase transitions is discussed by means of the local nature of the structure.

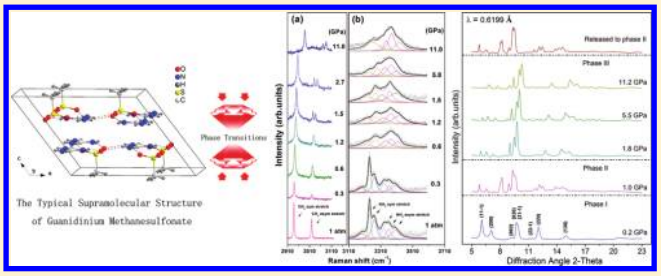

INTRODUCTION

Supramolecular chemistry, defined as "chemistry beyond the molecule" by Lehn, is an interdiscipline subject that concerns design, preparation, and applications of complex organized assemblies.[1] There has been tremendous interest in synthesis and characterization of novel supramolecular architectures with desirable properties, including host materials,[2] capsules, and switches.[3−5] Importantly, the supramolecular interactions, including hydrogen-bonding, π-stacking, van der Waals, and electrostatic interactions, are critical factors that govern self-organization and mechanical properties of supramolecular motifs. The thorough knowledge of cooperativity of non-covalent interactions within supramolecular motifs is crucial for understanding the mechanisms of assemblies and crystal engineering. Pressure is a significant thermodynamic variable and has been extensively applied to investigate structural stabilities.[6−10] More importantly, pressure is considered as a powerful tool to generate new structures and new properties, such as superhard materials and high-Tc superconductors.[11−14] Recently, pressure has been employed to explore the stability of supramolecular motifs, and rich phenomena have been investigated under high-pressure conditions, such as reversible pressure-induced amorphization (PIA),[15] distortions of hydrogen bonds,[16] rearrangements of hydrogen bonds, and phase transitions.[17−21] Especially, the cooperativity between hydrogen-bonding and π-stacking interactions in ammonium squarate has been studied.[22] The first phase transition at 2.7 GPa arises from rearrangements of hydrogen-bonded networks without significant changes of π-stacking interactions, while the second one is governed by π-stacking. All of the aforementioned experimental results demonstrate that pressure can be used as a powerful tool to explore the nature of noncovalent interactions and the corresponding cooperativity, which are expected to unravel the underlying mechanisms of molecular assemblies. Judicious investigations toward this aspect can in turn offer a valuable means to develop new strategies for controlling assemblies of building blocks and for further development of functionalized supramolecular motifs.

Supramolecular architectures based on guanidinium cation $C(NH_2)_3^+$ and sulfonate anions RSO_3^- occupy an important position in the supramolecular chemistry area. Hundreds of layered guanidinium motifs have been synthesized on the basis of monosulfonate and disulfonate anions.[23−27] The integrity of a hydrogen-bonded sheet is attributed to the maximization of hydrogen bonds between six electron lone pairs on sulfonate oxygen atoms and six guanidinium protons,[28] as well as electrostatic interactions between oppositely charged ions. This robustness is the predominant factor responsible for assemblies of guanidinium sulfonates and endows them with shaped and sized inclusion cavities.[29−31] The persistence of hydrogen bonds in guanidinium motifs has been observed even in the smectic state.[32] The lamellar guanidinium sulfonate host frameworks prove to have the potential for crystallization-based separation via selective inclusion.[33] Furthermore, the control of laser dyes aggregation in the guanidinium host frameworks can lead to the regulation of optical properties.[34,35]

Received: December 22, 2011
Revised: February 12, 2012
Published: February 16, 2012

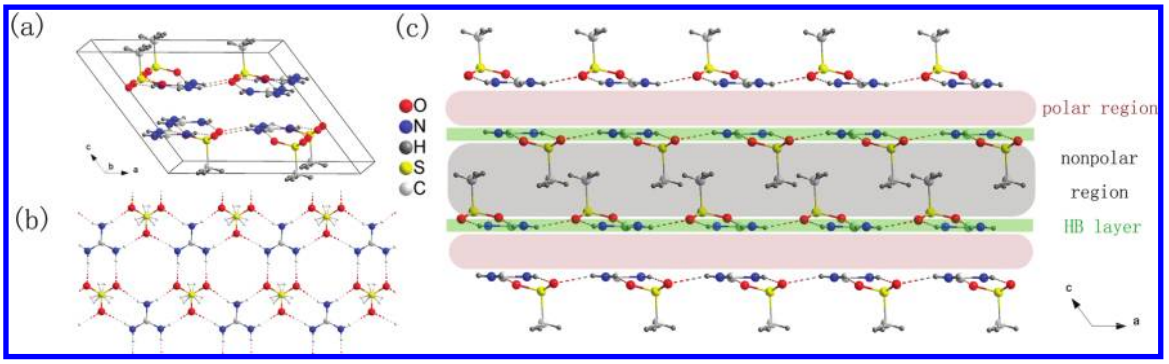

Figure 1. Crystal structure of GMS under ambient conditions: (a) the unit cell; (b) the hydrogen-bonded (HB) layer; (c) the view along HB layers. The hydrogen bonds are denoted by dashed lines. The hydrogen atoms of methyls are disordered over two positions.

Recently, ferroelectric phases of guanidinium sulfonates and other simple guanidinium-based motifs have been observed.[36−39] In spite of the aforementioned features, there is little work concerning mechanical properties of guanidinium sulfonates. Herein, we choose guanidinium methanesulfonate ($C(NH_2)_3^+ \cdot CH_3SO_3^-$, GMS) as an ideal model to investigate the structural properties of guanidinium sulfonate motifs under high-pressure conditions owing to its simpleness. Under ambient conditions, it crystallizes in the monoclinic space group $C2/m$ with $Z = 4$ in a unit cell;[40] the unit cell parameters are a = 12.778(5) Å, b = 7.342(2) Å, c = 9.998(2) Å, and β = 126.96(2)°. As shown in Figure 1, GMS presents the typical bilayered structure. The two-dimensional (2D) hydrogen-bonded sheet assembles into bilayers as a nonpolar region in which the methyl groups hold the sheets together via van der Waals interactions. The stacking sequence of bilayers comprises a polar region in which electrostatic and weaker dispersion interactions dominant. Therefore, the knowledge of high-pressure behavior of GMS is expected to provide new insights into the nature of hydrogen-bonding, electrostatic, and van der Waals interactions.

In this paper, we carried out in situ high-pressure Raman scattering and synchrotron X-ray diffraction (XRD) of GMS up to 11.0 and 11.2 GPa, respectively. Raman scattering and synchrotron XRD techniques have been extensively employed to monitor responses of materials to high pressures. Special attention is paid to the vibrations related to hydrogen bonding and methyl groups. This work aims to provide new insight into the cooperativity of hydrogen-bonding, electrostatic, and van der Waals interactions, which is expected to dominant high-pressure behaviors of the title compound. The analysis of phase transitions, as well as the cooperativity of the intermolecular interactions, has been performed.

EXPERIMENTAL SECTION

Single crystals of GMS were obtained by slow evaporation of stoichiometric methanol solution of guanidine hydrochloride and methanesulfonic acid.[40] The identity and crystallinity of GMS were confirmed by the conventional powder XRD because there was no diffraction signal from impurities in the pattern. The flawless crystals were selected and grinded to powder with grain size about several micrometers. The high-pressure Raman scattering and synchrotron X-ray diffraction experiments were performed with the polycrystalline form. The experiments on GMS powder were conducted in a symmetric diamond anvil cell (DAC) furnished with 500 μm culet diamonds. The powder was placed in the 160 μm diameter holes of the T301 steel gasket, which was preindented to the thickness of 60 μm. A small ruby chip was inserted into the sample compartment for in situ pressure calibration, utilizing the R1 ruby fluorescence method.[41] The 4:1 mixture of methanol and ethanol was used as pressure-transmitting medium (PTM). The hydrostatic-pressure condition around the powder was obtained based on Pascal principle and demonstrated by monitoring widths and separation of R1 and R2 lines. All of the experiments were conducted at room temperature.

Raman scattering measurements were performed with a Jobin Yvon HR800 microspectrometer using the 514.5 nm line as incident light. A 50× micro-objective was applied to regulate the position of the focused beam on the sample precisely. Raman spectra were recorded using a multiple track CCD detector with backscattering configuration. The laser power was 20 mW at the sample, and the integration time was 10 s. The standard silicone line was used for instrumental calibration before each experiment. The resolution of Raman system was about 1 cm^{-1}. The scattering patterns were analyzed using a combination of Lorentz and Gaussian functions.

In situ angle-dispersive X-ray diffraction (ADXRD) experiments were carried out on 4W2 beamline at High Pressure Station of Beijing Synchrotron Radiation Facility (BSRF). The monochromatic wavelength of 0.6199 Å was used for data collection, and the incident beam size was 20 × 30 μm^2. The sample−detector distance and geometric parameters were calibrated using a CeO_2 standard. The image-plate area detector (Mar345) was utilized to record the typical Bragg diffraction rings. In light of the light atoms (C, H, N, and O) in GMS, we took 400 s as the average exposure time for each spectrum to maintain sufficient intensity. The recorded two-dimensional (2D) data were analyzed to yield plots of intensity versus 2θ with Fit2D software.[42] Further analysis of ADXRD spectra was undertaken using commercial Materials Studio 5.0 to gain possible space groups and accurate lattice parameters.

RESULTS AND DISCUSSION

All of the observed Raman modes of GMS appear to stem from intramolecular fundamentals of the comprising ions, $C(NH_2)_3^+$ and $CH_3SO_3^-$, and assigned according to the literature.[43,44] Figures 2 and 3 summarize the evolution of the lattice modes of GMS and the corresponding pressure dependence from 0 to 11.0 GPa. In this study, GMS exhibits three lattice modes marked by the arrows shown in Figure 2 under ambient conditions. The three modes display ordinary blue shifts up to 0.6 GPa, originating from the expected contraction of interionic

dx.doi.org/10.1021/jp212349h | J. Phys. Chem. B 2012, 116, 3092−3098

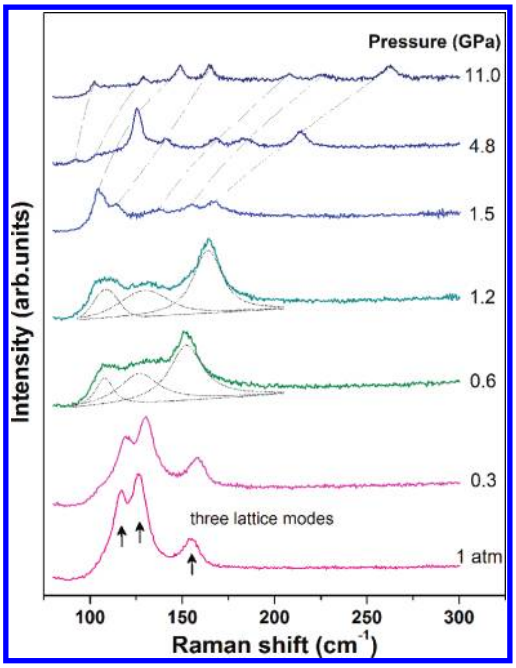

Figure 2. Selected Raman spectra of GMS ranging from 80 to 300 cm^{-1} under different pressures. Decomposition of the spectra and dashed lines are drawn for clarity.

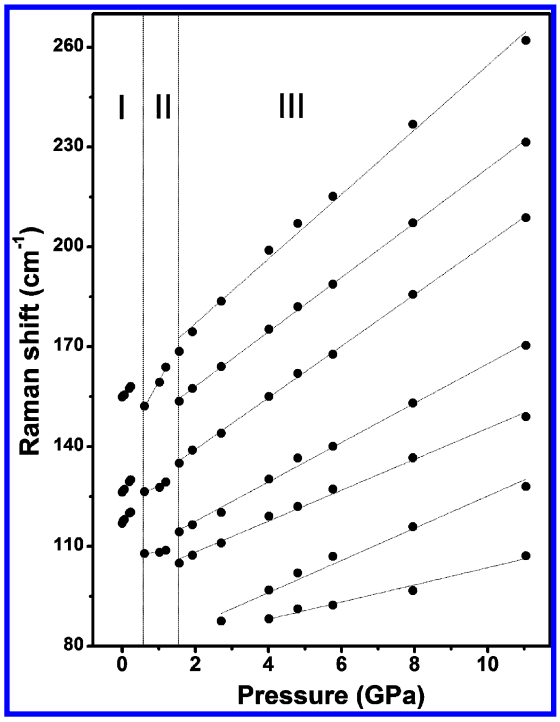

Figure 3. Peak positions of the lattice modes in the three phases as a function of pressure. Linear fits are performed for clarity. The vertical lines stand for boundaries of different phases.

distances with increasing pressure. At 0.6 GPa, a new set of lattice modes emerges, indicating that GMS undergoes a phase transition from phase I to phase II. Because the pattern at 0.6 GPa and the one at 0.3 GPa are essentially distinct, this phase transition seems to be reconstructive and will be discussed later. The three new modes gradually shift to high wavenumbers without any discontinuities on compression to 1.5 GPa, implying phase II exists in the pressure range of 0.6−1.5 GPa. At 1.5 GPa, another set of lattice modes is observed, indicative of the second transition from phase II to phase III. The evolution of the lattice modes in phase III does not reveal any remarkable changes from 1.5 to 11.0 GPa, suggesting phase III is stable up to 11.0 GPa, the highest pressure of this experiment. Figure 3 gives the pressure dependence of the lattice modes in the three phases. As can be seen, there are two obvious discontinuities at 0.6 and 1.5 GPa, respectively, consistent with two aforementioned phase transitions. Furthermore, the average pressure coefficients of lattice modes in three phases are 14.9, 8.7, and 6.2 cm^{-1}/GPa, respectively. These large coefficients imply interionic distances are easy to be shortened. This phenomenon is common among supramolecular materials because noncovalent interactions can be easily compressed compared with covalent bonds due to the weaker strengths in nature.[45]

Figure 4 depicts selected Raman spectra representing internal modes of GMS in the ranges 310−1120 cm^{-1} and 1400−1480 cm^{-1}. From ambient pressure to 0.6 GPa, all of the observed internal modes display normal blue shifts arising from the contraction of interatomic distances with increasing pressure. At 0.6 GPa, several significant changes in the spectrum, comprising the splitting of SO_3 twisting, CN_3 symmetric stretching, and CH_3 asymmetric deformation modes, demonstrate that GMS experiences a phase transition at this pressure. The pattern at 0.6 GPa retains unchanged all the way up to 1.5 GPa except the expected normal blue shifts, implying phase II is stable in the 0.6−1.5 GPa range. There are some remarkable changes related to the guanidinium cation and the methanesulfonate anion in the spectrum at 1.5 GPa. This pattern stays the same up to 11.0 GPa in essence, and therefore, phase III is stable in the range 1.5−11.0 GPa.

The pressure dependence of the internal modes ranging from 300 to 1500 cm^{-1} is illustrated in Figure 5. The discontinuities at 0.6 and 1.5 GPa are attributed to the two proposed phase transitions. Importantly, the modes assigned to CS stretching and CH_3 rocking shift to lower wavenumbers through the second phase transition. The red shifts imply the C−S distance is extended through the phase transition. However, the crystal structure tends to achieve close packing at high pressures. Therefore, these abnormal red shifts are expected to stem from the local distortion of methyl groups. In addition, the abrupt change with respect to CH_3 asymmetric deformation mode is also indicative of the distortion. These experimental results suggest the methyl group may evolve into a distorted state, which can lead to the softening of CS stretching and CH_3 rocking modes. This process is expected to be responsible for the abrupt red shifts of the two modes at 1.5 GPa. In other words, the second phase transition is proposed to be associated with local distortions of methyl groups.

Typical Raman spectra in the ranges 2910−3120 cm^{-1} and 3110−3600 cm^{-1} and the pressure dependence of corresponding modes are shown in Figures 6 and 7, respectively. The two CH_3 stretching modes reveal blue shifts owing to the repulsive nature of the chemical environment around the methyl groups below 0.6 GPa. The NH stretching modes exhibit the overall red shifts in the range 0−0.6 GPa, implying the hydrogen bonds in phase I are of weak or moderate type.[46] The contraction of interionic distances can reduce the separation between a hydrogen atom and an oxygen atom, which leads to enhancing the electrostatic attraction between them. This process can extend N−H distance, resulting in the red shifts of NH stretching modes. At 0.6 GPa, there is a pronounced

dx.doi.org/10.1021/jp212349h | J. Phys. Chem. B 2012, 116, 3092−3098

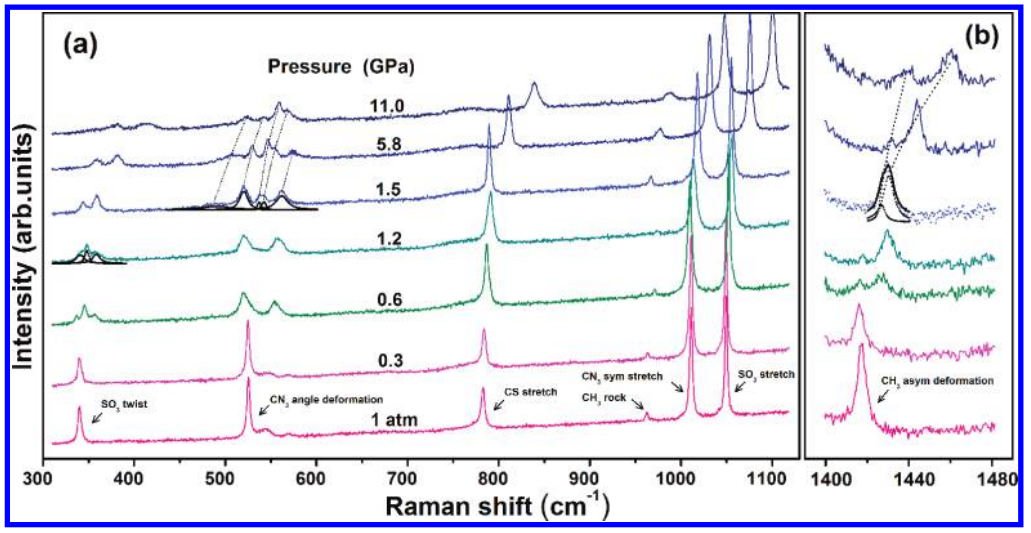

Figure 4. Evolution of Raman spectra of GMS at high pressures in the ranges (a) 310−1120 cm^{-1} and (b) 1400−1480 cm^{-1}. Decomposition of the spectra and dashed lines are performed for clarity.

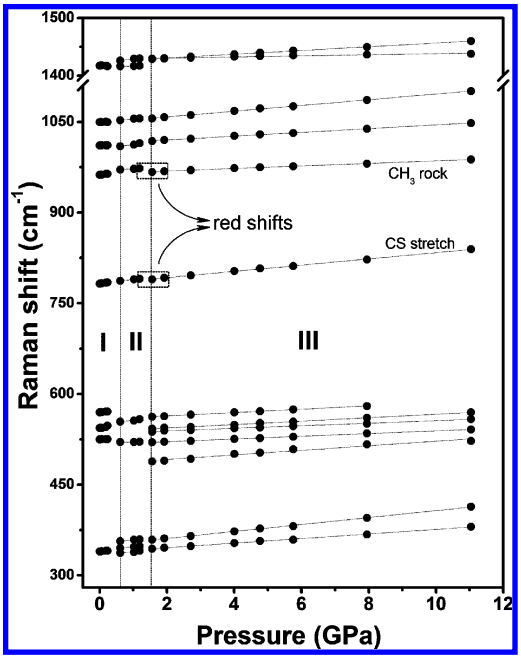

Figure 5. Frequency shifts of major internal modes ranging from 300 to 1500 cm^{-1} as a function of pressure. The vertical lines denote the boundaries of different phases.

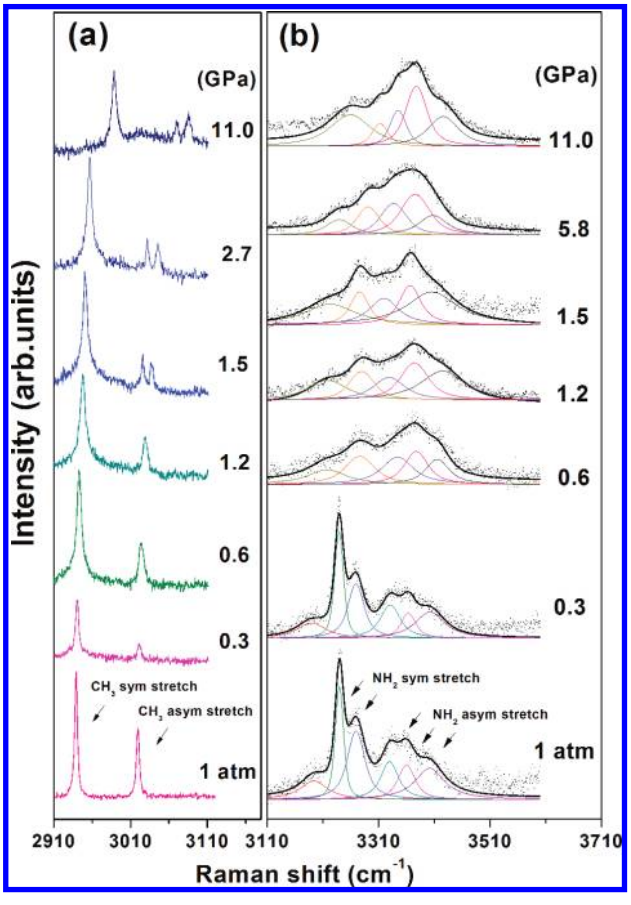

Figure 6. Selected Raman spectra of GMS at different pressures in (a) the range 2910−3120 cm^{-1} and (b) the NH stretching region. Decompositions of the NH stretching region are conducted for clarity.

redistribution in position and intensity in the NH stretching region, suggesting that the connectivity of hydrogen-bonded networks of guanidinium cations and methanesulfonate anions has been changed. Hence, the first phase transition may involve reconstruction of the two building blocks. Importantly, the redistribution of NH stretching modes at 0.6 GPa is similar with the evolution of NH stretching modes of guanidinium nitrate at ∼1 GPa.[18] This indicates the mechanisms for the phase transitions of GMS at 0.6 GPa and guanidinium nitrate at ∼1 GPa are similar. Therefore, the phase transition of GMS at 0.6 GPa may involve collapse of 2-dimensional N−H···O bonded sheets, and phase II is expected to be of 3-dimensional N−H···O bonded supramolecular motif.[19] In the 0.6−1.5 GPa range, the NH stretching modes display different high-pressure behaviors (red or blue shift) due to variations in the strength of the hydrogen bonds, whereas the CH_3 stretching modes show normal blue shifts only. At 1.5 GPa, the splitting of CH_3 asymmetric stretching mode was traced, while the NH stretching modes do not involve any significant changes. Furthermore, the NH stretching patterns above 1.5 GPa are identical to those in phase II. These results demonstrate the second phase transition is not reconstructive and related to the

dx.doi.org/10.1021/jp212349h | J. Phys. Chem. B 2012, 116, 3092−3098

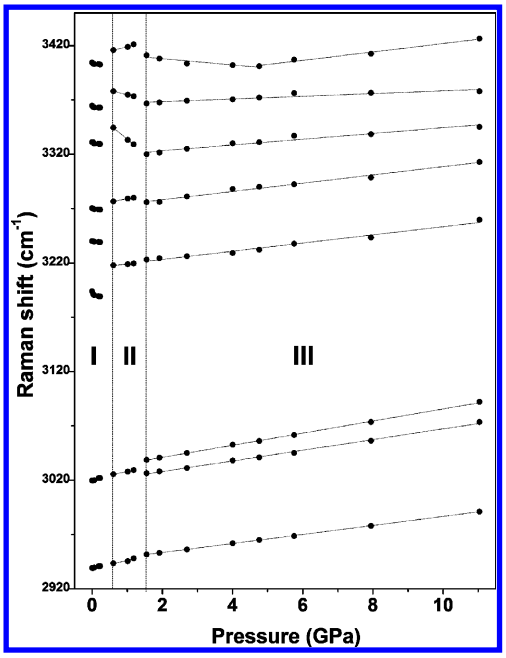

Figure 7. Frequency shifts of internal modes in the range 2900−3600 cm^{-1} as a function of pressure. The vertical lines represent the boundaries of different phases.

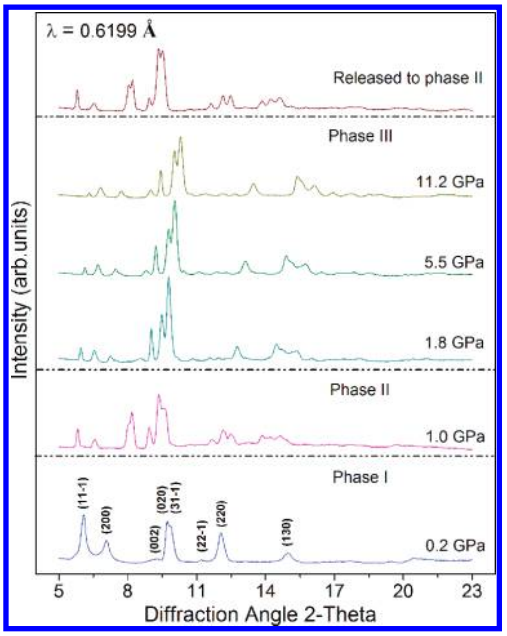

Figure 8. Representative synchrotron X-ray diffraction patterns of GMS at high pressures (with background subtracted). The upper pattern indicates GMS is retrieved to phase II on complete decompression.

distortions of methyl groups, consistent with the conclusion drawn from the evolution of CS stretching and CH_3 rocking modes. Above 1.5 GPa, the CH_3 stretching and NH stretching modes do not display any discontinuities up to 11.0 GPa, indicative of the stability of phase III over this pressure range. The two discontinuities at 0.6 and 1.5 GPa in Figure 7 are in line with the two proposed phase transitions. Therefore, we draw the conclusion that the first phase transition is reconstructive and the second one is associated with local distortions of methyl groups based on the above comments.

To gain straightforward evidence and more information about the phase transitions, we performed synchrotron ADXRD experiments. Figure 8 presents the dependence of typical diffraction patterns of GMS as a function of pressure up to 11.2 GPa. As can be seen, the pattern at 1.0 GPa is quite distinct from the one of the ambient phase, signifying the transition from phase I to phase II. More importantly, the diffraction patterns of the two phases exhibit different characteristics, such as peak positions and intensity distribution, suggesting the crystal structures of the two phases are not closely related. In other words, the first phase transition is reconstructive and involves the rearrangements of guanidinium cations and methanesulfonate anions. This is in accordance with the conclusion drawn from the Raman spectra. As shown in Figure 9, the diffraction pattern for the retrieved sample can be well indexed with *Pnma* symmetry, and the refined lattice parameters are a = 10.65(6) Å, b = 7.94(8) Å, c = 7.44(5) Å, and V = 630.51(4) Å^3. Therefore, we propose the space group of phase II is *Pnma*. With further compression, the new set of diffraction pattern at 1.8 GPa implies phase II of GMS has gone through a transition to phase III. The similarity of the XRD patterns at 1.0 and 1.8 GPa indicates the structures of the two phases are closely correlated. This result further demonstrates the conclusion drawn from Raman spectroscopy that the second phase transition is not reconstructive and can be ascribed to the distortion of the geometry of methyl groups. The diffraction peaks of phase III shift to higher angles with

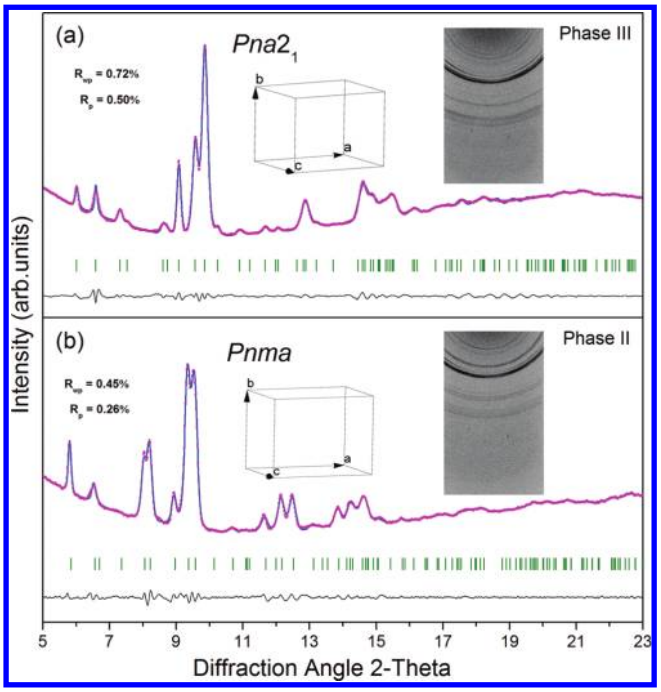

Figure 9. Pawley refinements of GMS with respect to (a) the pattern at 2.7 GPa and (b) the pattern after releasing the pressure. The refinements were conducted with the background. The black lines denote the difference between the observed (red) and the simulated (blue) profiles. The insets represent corresponding diffraction images.

increasing pressure as a result of the expected contraction of interatomic distances. No distinct change in the diffraction patterns is observed with further compression, proving phase III to be stable up to the pressure of 11.2 GPa. The Pawley refinement of the pattern at 2.7 GPa reveals that the space group *Pna*2$_1$ matches the diffraction data very well (Figure 9a). Hence, phase III is proposed to possess *Pna*2$_1$ symmetry, and

dx.doi.org/10.1021/jp212349h | J. Phys. Chem. B 2012, 116, 3092−3098

the indexed parameters are a = 9.70(5) Å, b = 7.42(5) Å, c = 7.82(4) Å, and V = 563.82(7) Å^3. The two phase transitions are not correlated with a loss of crystallinity, since the diffraction peaks do not broaden obviously across the phase transitions. Additionally, GMS is quenched to phase II upon complete decompression, implying the first phase transition is irreversible and the second one is reversible.

Hydrogen-bonding, electrostatic, and van der Waals interactions are predominant cohesive factors in the ambient structure of GMS. The two phase transitions can be interpreted in terms of the unique bilayered structure and the delicate cooperativity of the noncovalent interactions. On one hand, the interionic distances between guanidinium cations and methanesulfonate anions within each sheet are reduced with increasing pressure, leading to enhancement of hydrogen-bonding and electrostatic interactions accordingly.[47] This process can make a contribution to an increase of total Gibbs free energy. On the other hand, the electrostatic interactions between adjacent bilayers are strengthened because the separation between adjacent bilayers is shortened necessarily on compression, resulting in an increase of free energy. Concurrently, van der Waals interactions within nonpolar regions are expected to get enhanced as a result of contraction between methyl groups with increasing pressure. All of the aforementioned processes can destabilize the 2D hydrogen-bonded networks and trigger subtle translation of the sheets.[48] As a consequence, the bilayered structure cannot support the increase of Gibbs free energy anymore with compression, allowing for the rearrangements of hydrogen-bonded connectivities. This can account for the first phase transition at 0.6 GPa. With further compression from 0.6 to 1.5 GPa, the building blocks of GMS are brought much closer to achieve close packing within the same crystal symmetry. Overall, the chemical environments around each entire ion are repulsive in nature, evidenced by overall blue shifts of internal modes except the NH stretching modes participating in weak and moderate hydrogen bonds. This process can cause the Gibbs free energy to increase rapidly. Consequently, GMS adopts another crystal symmetry to release the increased free energy at 1.5 GPa, accompanied by the distortions of the methyl groups. In other words, the second phase transition stems from competition between flexibility of building blocks and dense packing. This flexibility is responsible for the reversibility of the second phase transition.

The proposed mechanisms for the phase transitions are favored by both Raman and ADXRD data. The reconstructive phase transition at 0.6 GPa is confirmed by remarkable redistribution in position and intensity relating to NH stretching modes. Meanwhile, the diffraction patterns of phases I and II are totally different, and further analysis reveals that the two phases belong to different crystal systems. The evolution of NH stretching modes is identical from 0.6 to 11.0 GPa except a small discontinuity in the plots of mode positions versus pressure. This suggests that the hydrogen-bonded connectivities retain the same in essence through the second phase transition even though there is a subtle distortion with respect to the hydrogen-bonded networks. Concurrently, the abrupt red shifts of CS stretching and CH_3 rocking vibrations, as well as the splitting of CH_3 asymmetry stretching mode, indicate methyl groups have experienced a distorted change over 1.5 GPa. Therefore, the second phase transition at 1.5 GPa is nonreconstructive and associated with the distortions of methyl groups. However, further neutron diffraction experiments are expected to give precise positions of hydrogen atoms.

CONCLUSION

The high-pressure behaviors of GMS have been examined using in situ Raman scattering and synchrotron XRD methods. Two phase transitions at 0.6 and 1.5 GPa are identified and analyzed. The transition from phase I to phase II is reconstructive and involves rearrangements of guanidinium cations and methanesulfonate anions. Analysis of ADXRD results implies phase II has *Pnma* symmetry. The second phase transition is nonreconstructive, whereas methyl groups have proven to evolve into a distorted state at 1.5 GPa. Further analysis of ADXRD results demonstrates phase III possesses $Pna2_1$ symmetry. In addition, the second phase transition is reversible while the first one is irreversible. High-pressure investigations of supramolecular motifs can provide new insight into delicate cooperativity of various noncovalent interactions and are of great significance to crystal engineering.

AUTHOR INFORMATION

Corresponding Author

*E-mail: zoubo@jlu.edu.cn.

Notes

The authors declare no competing financial interest.

ACKNOWLEDGMENTS

The authors are grateful to Prof. Jing Liu for help on experiments. This work is supported by NSFC (Nos. 21073071, and 51025206), and the National Basic Research Program of China (No. 2011CB808200) and Changjiang Scholar and Innovative Research Team in University (No. IRT1132). This work was conducted at 4W2 HP-Station, Beijing Synchrotron Radiation Facility (BSRF) which is supported by Chinese Academy of Sciences (Grant No. KJCX2-SW-N20, KJCX2-SW-N03).

REFERENCES

(1) Lehn, J. M. *Science* **1985**, *227*, 849.
(2) Jiao, D.; Biedermann, F.; Tian, F.; Scherman, O. A. *J. Am. Chem. Soc.* **2010**, *132*, 15734.
(3) Liu, Y.; Ward, M. D. *Cryst. Growth Des.* **2009**, *9*, 3859.
(4) Choudhury, S. D.; Mohanty, J.; Pal, H.; Bhasikuttan, A. C. *J. Am. Chem. Soc.* **2010**, *132*, 1395.
(5) Uno, S.; Dohno, C.; Bittermann, H.; Malinovskii, V. L.; Häner, R.; Nakatani, K. *Angew. Chem., Int. Ed.* **2009**, *121*, 7498.
(6) Okuchi, T.; Cody, G. D.; Mao, H. K.; Hemley, R. J. *J. Chem. Phys.* **2005**, *122*, 244509.
(7) Allan, D. R.; Blake, A. J.; Huang, D. G.; Prior, T. J.; Schröder, M. *Chem. Commun.* **2006**, *39*, 4081.
(8) Boldyreva, E. V. *Acta Crystallogr. A* **2008**, *64*, 218.
(9) Orgzall, I.; Emmerling, F.; Schulz, B.; Franco, O. *J. Phys.: Condens. Matter* **2008**, *20*, 295206.
(10) Murli, C.; Song, Y. *J. Phys. Chem. B* **2010**, *114*, 9744.
(11) Vepřek, S. *J. Vac. Sci. Technol. A* **1999**, *17*, 2401.
(12) McMillan, P. F. *Nat. Mater.* **2002**, *1*, 19.
(13) Imai, T.; Ahilan, K.; Ning, F. L.; McQueen, T. M.; Cava, R. J. *Phys. Rev. Lett.* **2009**, *102*, 177005.
(14) Medvedev, S.; McQueen, T. M.; Troyan, I.; Palasyuk, T.; Eremets, M. I.; Cava, R. J.; Naghavi, S.; Casper, F.; Ksenofontov, V.; Wortmann, G.; Felser, C. *Nat. Mater.* **2009**, *8*, 630.
(15) Wang, K.; Duan, D. F.; Wang, R.; Lin, A. L.; Cui, Q. L.; Liu, B. B.; Cui, T.; Zou, B.; Zhang, X.; Hu, J. Z.; Zou, G. T.; Mao, H. K. *Langmuir* **2009**, *25*, 4787.

(16) Li, S. R.; Li, Q.; Wang, K.; Tan, X.; Zhou, M.; Li, B.; Liu, B. B.; Zou, G. T.; Zou, B. *J. Phys. Chem. B* **2011**, *115*, 11816.
(17) Mishra, A. K.; Murli, C.; Garg, N.; Chitra, R.; Sharma, S. M. *J. Phys. Chem. B* **2010**, *114*, 17084.
(18) Wang, R.; Li, S. R.; Wang, K.; Duan, D. F.; Tang, L. Y.; Cui, T.; Liu, B. B.; Cui, Q. L.; Liu, J.; Zou, B.; Zou, G. T. *J. Phys. Chem. B* **2010**, *114*, 6765.
(19) Katrusiak, A.; Szafrański, M.; Podsiadlo, M. *Chem. Commun.* **2011**, *47*, 2107.
(20) Wang, K.; Duan, D. F.; Wang, R.; Liu, D.; Tang, L. Y.; Cui, T.; Liu, B. B.; Cui, Q. L.; Liu, J.; Zou, B.; Zou, G. T. *J. Phys. Chem. B* **2009**, *113*, 14719.
(21) Martins, D. M. S.; Middlemiss, D. S.; Pulham, C. R.; Wilson, C. C.; Weller, M. T.; Henry, P. F.; Shankland, N.; Shankland, K.; Marshall, W. G.; Ibberson, R. M.; Knight, K.; Moggach, S.; Brunelli, M.; Morrison, C. A. *J. Am. Chem. Soc.* **2009**, *131*, 3884.
(22) Li, S. R.; Wang, K.; Zhou, M.; Li, Q.; Liu, B. B.; Zou, G. T.; Zou, B. *J. Phy. Chem. B* **2011**, *115*, 8981.
(23) Russell, V. A.; Evans, C. C.; Li, W.; Ward, M. D. *Science* **1997**, *276*, 575.
(24) Holman, K. T.; Martin, S. M.; Parker, D. P.; Ward, M. D. *J. Am. Chem. Soc.* **2001**, *123*, 4421.
(25) Holman, K. T.; Pivovar, A. M.; Ward, M. D. *Science* **2001**, *294*, 1907.
(26) Horner, M. J.; Holman, K. T.; Ward, M. D. *J. Am. Chem. Soc.* **2007**, *129*, 14640.
(27) Soegiarto, A. C.; Comotti, A.; Ward, M. D. *J. Am. Chem. Soc.* **2010**, *132*, 14603.
(28) Zheng, W. T.; Sun, C. Q. *Prog. Solid State Chem.* **2006**, *34*, 1.
(29) Swift, J. A.; Pivovar, A. M.; Reynolds, A. M.; Ward, M. D. *J. Am. Chem. Soc.* **1998**, *120*, 5887.
(30) Evans, C. C.; Sukarto, L.; Ward, M. D. *J. Am. Chem. Soc.* **1999**, *121*, 320.
(31) Horner, M. J.; Holman, K. T.; Ward, M. D. *Angew. Chem., Int. Ed.* **2001**, *40*, 4045.
(32) Mathevet, F.; Masson, P.; Nicoud, J.-F.; Skoulios, A. *Chem.—Eur. J.* **2002**, *8*, 2248.
(33) Pivovar, A. M.; Holman, K. T.; Ward, M. D. *Chem. Mater.* **2001**, *13*, 3018.
(34) Burke, N. J.; Burrows, A. D.; Mahon, M. F.; Teat, S. J. *CrystEngComm* **2004**, *6*, 429.
(35) Soegiarto, A. C.; Ward, M. D. *Cryst. Growth Des.* **2009**, *9*, 3803.
(36) Szafrański, M.; Katrusiak, A. *Phys. Rev. B* **2006**, *73*, 134111.
(37) Szafrański, M. *J. Phy. Chem. B* **2011**, *115*, 8755.
(38) Szafrański, M.; Jarek, M. *J. Phy. Chem. B* **2008**, *112*, 3101.
(39) Szafrański, M. *J. Phy. Chem. B* **2011**, *115*, 10277.
(40) Russell, V. A.; Etter, M. C.; Ward, M. D. *J. Am. Chem. Soc.* **1994**, *116*, 1941.
(41) Mao, H. K.; Bell, P. M.; Shaner, J. W.; Steinberg, D. J. *J. Appl. Phys.* **1978**, *49*, 3276.
(42) Hammersley, A. P.; Svensson, S. O.; Hanfland, M.; Fitch, A. N.; Hausermann, D. *High Pressure Res.* **1996**, *14*, 235.
(43) Durig, J. R.; Zhou, L.; Schwartz, T.; Gounev, T. *J. Raman Spectrosc.* **2000**, *31*, 193.
(44) Sension, R. J.; Hudson, B.; Callis, P. R. *J. Phys. Chem.* **1990**, *94*, 4015.
(45) Johnson, E. R.; Keinan, S.; Mori-Sánchez, P.; Contreras-García, J.; Cohen, A. J.; Yang, W. *J. Am. Chem. Soc.* **2010**, *132*, 6498.
(46) Hamann, S. D.; Linton, M. *Aust. J. Chem.* **1976**, *29*, 1825.
(47) Katrusiak, A.; Szafrański, M. *J. Mol. Struct.* **1996**, *378*, 205.
(48) Martin, S. M.; Yonezawa, J.; Horner, M. J.; Macosko, C. W.; Ward, M. D. *Chem. Mater.* **2004**, *16*, 3045.